PHYSICAL REVIEW B **97**, 201104(R) (2018)

Rapid Communications

Direct observation of strain-induced orbital valence band splitting in $HfSe_2$ by sodium intercalation

T. Eknapakul,[1] I. Fongkaew,[1] S. Siriroj,[1] W. Jindata,[1] S. Chaiyachad,[1] S.-K. Mo,[2] S. Thakur,[3] L. Petaccia,[3]
H. Takagi,[4,5] S. Limpijumnong,[1,6] and W. Meevasana[1,6,*]
[1]*School of Physics, Suranaree University of Technology, Nakhon Ratchasima 30000, Thailand*
[2]*Advanced Light Source, Lawrence Berkeley National Laboratory, Berkeley, California 94720, USA*
[3]*Elettra Sincrotrone Trieste, Strada Statale 14 km 163.5, I-34149 Trieste, Italy*
[4]*Department of Physics, University of Tokyo, Hongo, Tokyo 113-0033, Japan*
[5]*Max-Planck Institute for Solid State Research, Heisenbergstrasse 1, D-70569 Stuttgart, Germany*
[6]*NANOTEC-SUT Center of Excellence on Advanced Functional Nanomaterials,*
Suranaree University of Technology, Nakhon Ratchasima 30000, Thailand

(Received 8 January 2018; revised manuscript received 23 March 2018; published 7 May 2018)

By using angle-resolved photoemission spectroscopy (ARPES), the variation of the electronic structure of $HfSe_2$ has been studied as a function of sodium intercalation. We observe how this drives a band splitting of the p-orbital valence bands and a simultaneous reduction of the indirect band gap by values of up to 400 and 280 meV, respectively. Our calculations indicate that such behavior is driven by the band deformation potential, which is a result of our observed strain induced by sodium intercalation. The applied uniaxial strain calculations based on density functional theory agree strongly with the experimental ARPES data. These findings should assist in studying the physical relationship between intercalation and strain, as well as for large-scale two-dimensional straintronics.

DOI: 10.1103/PhysRevB.97.201104

Transition-metal dichalcogenides (TMDs) have been extensively studied as they exhibit unique physical and electrical properties [1–4] with potential applications spanning nanoelectronics, optoelectronics, and valleytronics [3,5,6]. Thus far, most studies have been focused on semiconducting group-VIB TMDs ($2H$-MX_2 where M = Mo, W and X = S, Se) which hold enormous potential in creating novel electronic devices such as tunable optoelectronics and tunneling field-effect transistors [2,3,7–9]. Among more than 80 TMD compounds, the so-called "early TMDs" which adopt a tetragonal phase ($1T$) are less frequently investigated and hence much remains to be learned from them [10–13]. For instance, few semiconducting Hf-based TMDs have been reported featuring both a small band gap (ca. 1.13 eV) and a large work function approaching that of Si [14,15]. The synthesis of high-quality $HfSe_2$ has been achieved recently, e.g., $HfSe_2$ single crystals can be prepared by a chemical vapor transport technique [13] and nondistorted $HfSe_2$ thin films can be grown on many different substrates by molecular beam epitaxy, which can be used in the study of TMD heterointerfaces [16,17]. These compounds are predicted to be anisotropic with the highest electron mobility among TMDs approaching 2500 $cm^2\ V^{-1}\ s^{-1}$ [18], making it a great candidate for field-effect transistors and photovoltaic applications [15,18,19].

Alkali-metal intercalation achieved by surface electron doping is a powerful method for controlling the intrinsic properties in layered TMDs, due to the weak van der Waals interaction between neighboring chalcogen planes [20–22]. Charge accumulation plays an important role in filling the d orbitals of the transition metal, which results in electronic reconstruction. This leads to novel properties such as the appearance of charge density waves and superconductivity [11,23], and quasifreestanding layers [24–26].

The intercalation process affects not only the electronic structure but also the atomic structure, which is strongly coupled with external strain [27,28]. This relationship is evident from a body of research reporting doping- or strain-related characteristics such as phase transitions and optical phenomena (through, e.g., photoluminescence and Raman spectroscopy) [27,29,30]. Computational and experimental studies of strain engineering have significantly advanced in recent decades, exhibiting a wide tunability of the optical band gap, electronic structure, and magnetic properties by the introduction of measured degrees of strain [9,31–34]. Such electronic modification is rationalized by lattice deformation, which is occasioned by the variation of both strain and doping conditions [35,36]. Manipulation of the doping (intercalation)-strain relationship therefore holds promise for sophisticated device engineering, providing a combination of efficient electrolytic gating and lattice straining.

Valence band splitting in layered TMDs by spin-orbit coupling has been proposed to give noncenter splittings as observed in MoS_2, $MoSe_2$, and WSe_2 [24,37–39]. In contrast, calculated valence band splitting at the zone center can occur by applying external uniaxial strain as a result of a deformation potential [10,40]. However, direct observation of this phenomenon, a signature of a tunable orbital-valley degree of freedom, has yet to be reported. In this Rapid Communication, we investigate the influence of sodium intercalation on the electronic structure of $HfSe_2$ by using angle-resolved photoemission spectroscopy (ARPES). First, with sodium evaporated

---

[*] worawat@g.sut.ac.th

on the sample, electrons from sodium atoms are donated to HfSe$_2$. As a result of this donation, an upward shift of the Fermi level in the conduction band of HfSe$_2$ is expected [23]. Second, a strongly tunable valence band splitting is observed at the zone center, accompanied by band-gap shrinkage, each of which potentially arises due to lattice distortion by uniaxial strain [27,28]. Our density functional theory (DFT) calculations demonstrate the lattice distortion arising from sodium intercalation and hence the existence of uniaxial strain. The experimentally observed changes in electronic characteristics agree strongly with the calculated electronic structures under an applied uniaxial strain, which therefore supports claims for a strong relationship between intercalation and strain. These findings are critical in understanding the occurrence of uniaxial strain induced by chemical doping as well as establishing a different synthetic route to chemical gating and strain-engineered devices in layered TMDs.

Our 1T-HfSe$_2$ single crystals were grown using a flux growth method and cleaved in ultrahigh vacuum at pressures below 2×10^{-11} Torr, providing a pristine surface. The 1T-HfSe$_2$ layered structure resembles CdI$_2$, by featuring Se-Hf in octahedral coordination. Each Se layer within HfSe$_2$ is A-B stacked perpendicular to the c axis, sandwiched by Hf layers with lattice constants $a = 3.71$–3.74 Å and $c = 6.14$ Å [see Fig. 1(a)] [16,41]. Our ARPES measurements were performed at BL 10.0.1 of the Advanced Light Source (USA) and BL 10.2R BaDElPh of the Elettra Sincrotrone Trieste (ITA). The photon energies of s- and p-polarized light were set to be 20–80 eV with energy and angular resolution of 10–20 meV and 0.2°, respectively. The sample temperature was set to around 40–80 K. Surface sodium depositions were achieved using a SAES getter evaporation source.

Figures 1(b) and 1(c) show the ARPES measurement of the HfSe$_2$ electronic structure for the pristine and sodium-evaporated samples. The electronic structure of our pristine HfSe$_2$ along the M-Γ-K direction is comparable with the bulk, as obtained in previous experiments and calculations [10,17]. There are no electronic states located at the Fermi level, as expected from the semiconducting bulk [Fig. 1(b)]. Moreover, a nondegenerate valence band derived from one unit cell (two monolayers) labeled by v_1 and v_2 was observed, which can arise from a weak interlayer interaction [17,42]. After sufficient sodium deposition [Fig. 1(c)], the valence band shifts to a higher binding energy while an additional band (v_s) emerged at the Γ point, which is a result of an electron donation from the alkali metal to the host material [28]. The direct population leads to filling of the conduction band, which gives rise to an ellipsoidal Fermi contour, indicative of anisotropic behavior at all M points of the Brillouin zone and consistent with previous calculations [Fig. 1(d)] [10,18].

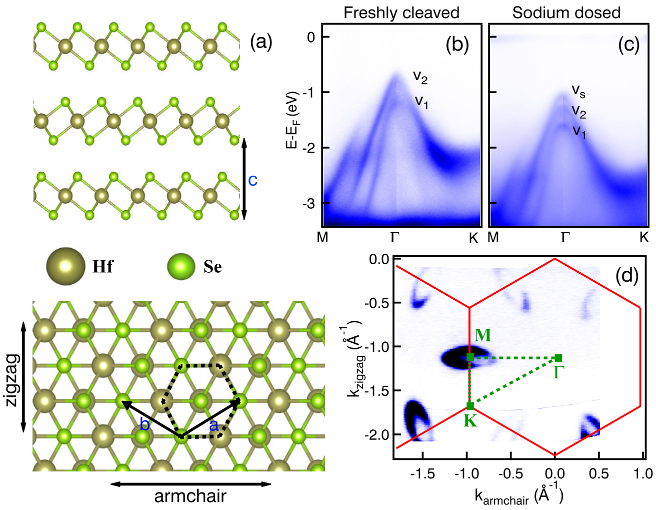

FIG. 1. (a) The side and top view atomic structure of 1T-HfSe$_2$. The dashed hexagon represents the in-plane unit cell. Electronic structure of HfSe$_2$ single crystal along the M-Γ-K direction of (b) freshly cleaved and (c) decent amounts of sodium evaporation, clearly indicates the chemical shift and valence band splitting at the Γ point. (d) Corresponding Fermi surface map of sodium-dosed sample.

We investigated the evolution of the HfSe$_2$ electronic structure as a function of electron doping, achieved by increasing the exposure time for sodium evaporation [with a constant current ($I = 6.2$ A)]. To avoid confusion between doping and intercalation, we define doping as the number of electrons that sodium atoms donate to HfSe$_2$ from both observed intercalation and adsorption. Doping concentration (or surface carrier density n_{2D}) can be calculated from its Luttinger area ($n_{2D} = g_v \frac{k_S k_L}{2\pi}$, where $g_v = 3$ is the valley multiplicity for all occupied ellipsoidal pockets, and k_S and k_L are short and long ellipsoidal radii). As shown in Figs. 2(a)–2(e), n_{2D} is observed to be increased upon an increase of exposure time. The maximum surface carrier density can reach 1.85×10^{14} cm^{-2} or approximately 0.27 electrons per surface unit cell higher than those previously reported [28,37]. This suggests that HfSe$_2$ has a high capacity for extrinsic dopant atoms via its van der Waals (vdW) layer, making it suitable as a host material or substrate. We found a clear increase in the valence band splitting ($E_{\text{split}} = v_s - v_2$) at the valence band maximum, found by fitting the energy distribution curves (EDCs) around the Γ point of two distinct valence bands up to 400 meV [Figs. 2(k)–2(o), as summarized in Fig. 2(p)]. By extracting the gap between the conduction band minimum [M point, Figs. 2(f)–2(j)] and valence band maximum [Γ point, Figs. 2(k)–2(o)], we found a continuous decrease in the indirect band gap up to a maximum splitting of 280 meV [Fig. 2(q)]. This observation could be ascribed to surface accumulation or intercalation caused by the introduction of the alkali metal at the surface. Note that the changes in conduction band are described in the Supplemental Material [43].

Unlike previous reports of alkali deposition on several TMDs [37,44], our observed band splitting cannot be explained by the introduction of a surface electric field from charge accumulation. For example, the existence of valence band splitting at the K point can be obtained by applying an electric field at the WSe$_2$ surface, but could not be seen at the Γ point of HfSe$_2$. This may be the critical difference between 1T and 2H symmetry [43]. In other words, the intercalation should be the dominant effect in HfSe$_2$ system and a rationale is needed to include strain here.

Based on the experimental findings, we then calculated the band structure of HfSe$_2$ under different strain conditions induced by sodium intercalation. Calculations were carried out within the framework of density functional theory with projector augmented wave potentials (PAW) [45] as

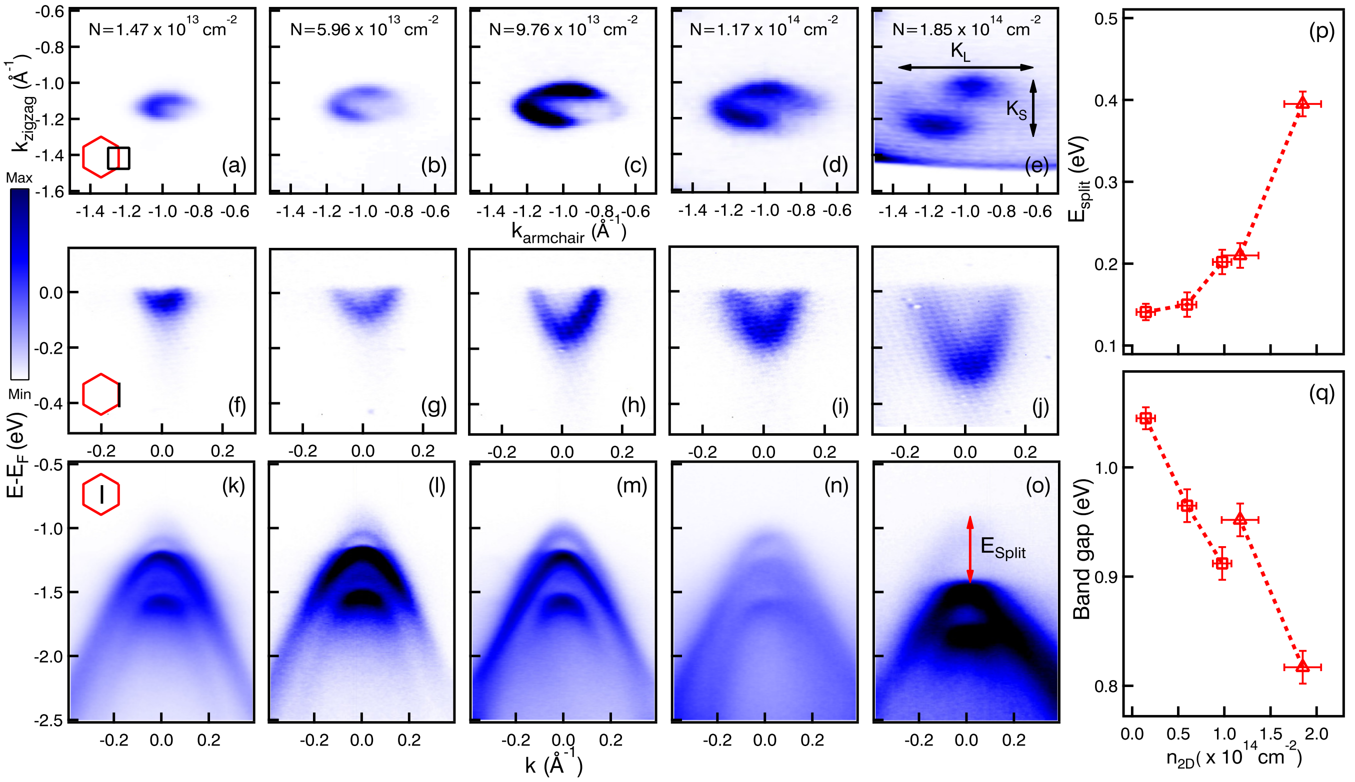

FIG. 2. (a)–(e) Occupied Fermi surface at the M point as a function of electron doping. (f)–(j) Corresponding two-dimensional Fermi pocket along the K-M-K direction. (k)–(o) Tunability of valence band splitting at the Γ point corresponding to (a)–(e). (p) Valence band splittings (E_{split}) and (q) extracted band-gap shrinkage as a function of electron doping. All data were taken at 60 eV photon energy.

implemented in the VASP code. The Perdew-Burke-Ernzerhof (PBE) approximation is used for the exchange correlation terms [46,47] with van der Waals corrections carried out using the DFT+D3 method [42].

The Fermi surface maps spanning three M points of the Brillouin zone of lightly and heavily doped samples are shown in Figs. 3(a) and 3(b), respectively. By using a $\bar{k}_{M\text{-}M}$ distance of 0.977 Å^{-1} (as given by $\frac{2\pi}{\sqrt{3}a}$) for a fresh sample to be used as a reference, we found Brillouin zone shrinkage up to 2.76%, as determined by a decreasing of $\bar{k}_{M\text{-}M}$ as a function of electron doping [Fig. 3(c)]. This could be rationalized by the intercalation of sodium into $\mathrm{HfSe_2}$ layers, hence enlarging the unit cell in real space [48,49]. Moreover, the Brillouin zone shrinkage appears larger in the reciprocal armchair direction than the zigzag direction, suggesting a preference for expansion in the armchair direction in real space. Figure 3(d) represents the possibility of introducing armchair tensile strain when adding sodium at the unit cell center. The fully relaxed atomic structure of $\mathrm{Na_{0.25}HfSe_2}$ illustrates the lattice distortion and expansion effects arising from the introduction of a single sodium atom into the center of a $2 \times 2 \times 2$ cell [43].

The calculated electronic band structure of anisotropic lattice distortion in $\mathrm{HfSe_2}$ is supported by the experimental ARPES results, where three different holelike bands are observed near the valence band maximum of $\mathrm{HfSe_2}$ arising from Se p_x, p_y, and p_z orbitals [10]. The most heavily “holelike” band is p_z, followed by p_x then p_y. Figures 3(e) and 3(f) illustrate the schematic band evolution arising from external uniaxial strain. In $\mathrm{HfSe_2}$, the top of the valence band is contributed to by Se p orbitals, where p_x and p_y orbitals are degenerate at the valence band maximum, while the p_z orbital is located at slightly higher binding energy [Fig. 3(e)]. The relative positions of the orbitals can be rearranged by applying uniaxial strain. As shown in Fig. 3(f), the p_x orbital is shifted to a higher binding energy, resulting in the contribution of p_y to the valence band maximum under armchair tensile strain conditions. Light polarization-dependent measurements are best suited to reconciling orbital ordering with those bands expected within our geometry [50]. Figure 3(g) shows the electronic band structure measured by s polarization (s-pol) where the most intense bands are p_x orbitals. In contrast, p polarization (p-pol) measurement reveals more orbitals than s-pol, where p_y and p_z appear most notable [Fig. 3(h)]. Figure 3(i) shows the intensity difference obtained by subtracting s- and p-pol data, clearly indicating the valence band splitting of p_x and p_y orbitals in our doped sample. Overall, it is shown that sodium intercalation can lead to lattice distortion. The distorted $\mathrm{HfSe_2}$ prefers to rearrange in armchair tensile strain [51,52], as confirmed by our polarization-dependent ARPES data [Fig. 3(i)].

The Fermi surface area from the ARPES data suggests that sodium atoms donate an average of 0.27 electrons per surface unit cell, which is comparable to the computational $\mathrm{Na_{0.25}HfSe_2}$ model. The increase in the valence band splitting brought on by sodium intercalation is a result of an increased uniaxial strain in the doped $\mathrm{HfSe_2}$ layer. Electronic structure calculations for $\mathrm{HfSe_2}$ have been performed under armchair and zigzag uniaxial strains ranging from −5% to 5%. The

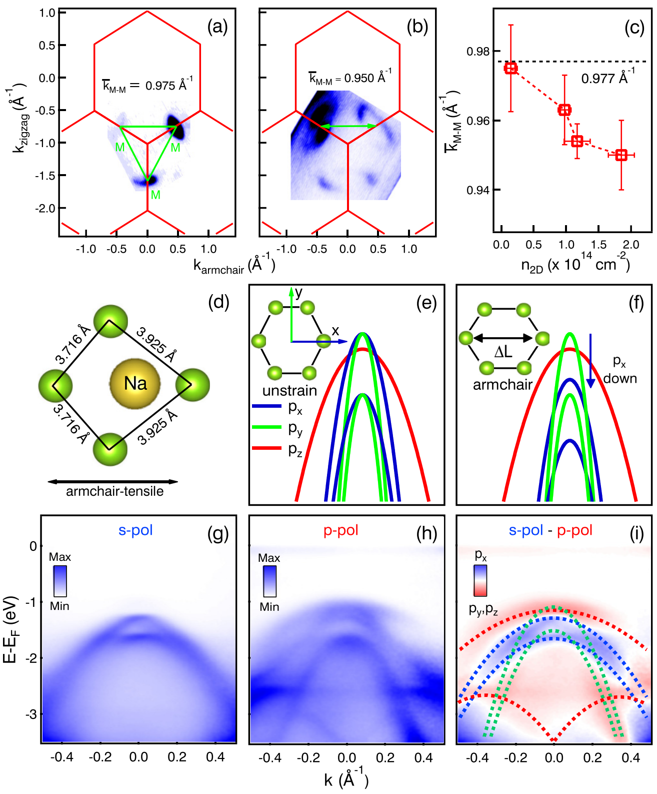

FIG. 3. (a) Fermi surface map spanning three M points of (a) lightly and (b) heavily sodium-doped surfaces. (c) Extracted $\bar{k}_{M\text{-}M}$ distance as a function of electron doping. (d) Schematic of armchair tensile strain caused by the addition of a sodium atom at the zone center. (e), (f) Schematic band dispersions near the valence band maximum indicate the degenerated band as well as band evolution by applying armchair tensile strain. Electronic band dispersion measured along the M-Γ-M direction with (g) s-polarized and (h) p-polarized light. (i) The difference in spectral weight between s and p polarization reveals the explicit orbital character near the valence band maximum.

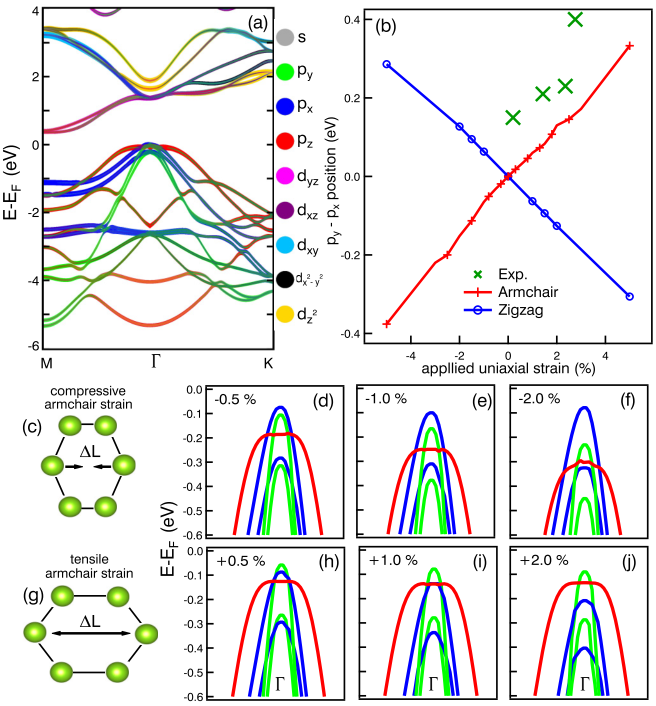

FIG. 4. (a) The calculated orbital projected band structure of HfSe$_2$ using DFT calculation+vdW correction. (b) Extracted valence band splitting ($p_y - p_x$), corresponding to ($v_s - v_2$) of the ARPES data as a function of applied uniaxial strain. Dominant electronic structure at the top of the valence band by varying between (c)–(f) compressive and (g)–(j) tensile armchair uniaxial strains.

unstrained orbital-projected electronic structure of HfSe$_2$ is shown in Fig. 4(a) representing Se p orbitals located at the top of the valence band. Figures 4(d)–4(j) represent the zoomed-in electronic structures around the Γ point between −2% and +2% uniaxial armchair strain, where minus and plus signs indicate compressive [Fig. 4(c)] and tensile [Fig. 4(g)] strain, respectively. The lattice deformation plays an important role in varying relative band positions (and therefore band gap) and valence band splittings in these calculations. The p_x (p_y) orbitals are shifted in energy monotonically while p_y (p_x) orbitals are essentially constant as a function of applied tensile (compressive) strain, resulting in an opposite sign of valence band splitting. Regarding the two previously mentioned in-plane p-orbital bands, which are degenerate at the valence band maximum for bulk HfSe$_2$, applying uniaxial strain significantly lifts the degeneracy and therein changes the electronic band gap. The calculated valence band splitting ($p_y - p_x$) reaches 333 and −376 meV in 5% tensile and compressive armchair strain, respectively. The calculation of applied zigzag uniaxial strain has been performed, yielding valence band splitting in the opposite direction [Fig. 4(b)]. Larger valence band splittings obtained from the ARPES data [green marks in Fig. 4(b)] were found as compared with the calculated tensile strain values. This may be describable by anisotropic lattice distortion in which the asymmetrically enlarged lattice (tensile armchair strain) is compressed in the zigzag direction to maintain its volume. Overall, however, we note that the observed orbital valence band splitting is generally consistent with armchair tensile strain.

In summary, we have observed an increase in orbital valence band splitting, band-gap shrinkage, and anisotropic unit cell enlargement by evaporating sodium onto HfSe$_2$ surfaces corresponding to 0.27 electrons per surface unit cell. Our experimental ARPES data are well supported by computational DFT calculations of fully relaxed Na$_{0.25}$HfSe$_2$, where the calculations showed the HfSe$_2$ layer anisotropically distorted with about 5% strain due to sodium intercalants. Overall, it can be concluded that the presence of effective armchair tensile strain is induced by sodium intercalation. We have also demonstrated the possibility of orbital control at the valence band maximum with "valley physics." In future work, this could be achieved by applying opposite uniaxial strain by introducing different cationic (Na, K) or anionic (Cl, Br) intercalants or ionic liquids. These observations support an overall understanding of intercalation/strain physics to facilitate the exploration of interesting phenomena among layered TMDs. This could also be used as a direct technique for large-scale strain engineering in tuning optical and electronic properties as well as for straintronics such as nanoscale stress sensors and tunable photonic devices [53,54].

We acknowledge P. D. C. King, P. Songsiririthigul, and T. Kongnok for helpful discussions. This work is supported by Thailand Research Fund (TRF) and Suranaree University of Technology (SUT) (Grant No. BRG5880010), Research Fund for DPST Graduate with First Placement (Grant No. 021/2555), and the Office of Naval Research Global under Grant No. N62909-18-1-2018. The computing resources were provided by Theoretical Computation Section, SLRI, Thailand. S.S. acknowledges the Royal Golden Jubilee Ph.D. Program (Grant No. PHD/0007/2555). We thank ALS and Elettra for the allocation of synchrotron radiation beamtimes. The Advanced Light Source is supported by the US Department of Energy under Contract No. DE-AC02-05CH11231.

---

[1] J. A. Wilson and A. D. Yoffe, Adv. Phys. **18**, 193 (1969).

[2] B. Radisavljevic, A. Radenovic, J. Brivio, V. Giacometti, and A. Kis, Nat. Nanotechnol. **6**, 147 (2011).

[3] S. H. Lee, S.-W. Min, Y.-G. Chang, M. K. Park, T. Nam, H. Kim, J. H. Kim, S. Ryu, and S. Im, Nano Lett. **12**, 3695 (2012).

[4] J. M. Riley, F. Mazzola, M. Dendzik, M. Michiardi, T. Takayama, L. Bawden, C. Granerød, M. Leandersson, T. Balasubramanian, M. Hoesch, T. K. Kim, H. Takagi, W. Meevasana, Ph. Hofmann, M. S. Bahramy, J. W. Wells, and P. D. C. King, Nat. Phys. **10**, 835 (2014).

[5] Q. H. Wang, K. Kalantar-Zadeh, A. Kis, J. N. Coleman, and M. S. Strano, Nat. Nanotechnol. **7**, 699 (2012).

[6] H. Zeng, J. Dai, W. Yao, D. Xiao, and X. Cui, Nat. Nanotechnol. **7**, 490 (2012).

[7] O. Lopez-Sanchez, D. Lembke, M. Kayci, A. Radenovic, and A. Kis, Nat. Nanotechnol. **8**, 497 (2013).

[8] B. Radisavljevic, M. B. Whitwick, and A. Kis, ACS Nano **5**, 9934 (2011).

[9] T. Shen, A. V. Penumatcha, and J. Appenzeller, ACS Nano **10**, 4712 (2016).

[10] H. Guo, N. Lu, L. Wang, X. Wu, and X. C. Zeng, J. Phys. Chem. C **118**, 7242 (2014).

[11] J. F. Zhao, H. W. Ou, G. Wu, B. P. Xie, Y. Zhang, D. W. Shen, J. Wei, L. X. Yang, J. K. Dong, M. Arita, H. Namatame, M. Taniguchi, X. H. Chen, and D. L. Feng, Phys. Rev. Lett. **99**, 146401 (2007).

[12] M. Chhowalla, H. S. Shin, G. Eda, L.-J. Li, K. P. Loh, and H. Zhang, Nat. Chem. **5**, 263 (2013).

[13] K. Radhakrishnan and M. Pilla, in *Proceedings of the IVth National Conference on Thermophysical Properties - NCTP'07*, edited by P. Predeep, S. Prasanth, and A. S. Prasad, AIP Conf. Proc. Vol. 1004 (AIP, Melville, NY, 2008), p. 283.

[14] S. Lebègue, T. Björkman, M. Klintenberg, R. M. Nieminen, and O. Eriksson, Phys. Rev. X **3**, 031002 (2013).

[15] C. Gaiser, T. Zandt, A. Krapf, R. Serverin, C. Janowitz, and R. Manzke, Phys. Rev. B **69**, 075205 (2004).

[16] R. Yue, A. T. Barton, H. Zhu, A. Azcatl, L. F. Pena, J. Wang, X. Peng, N. Lu, L. Cheng, R. Addou, S. McDonnell, L. Colombo, J. W. P. Hsu, J. Kim, M. J. Kim, R. M. Wallace, and C. L. Hinkle, ACS Nano **9**, 474 (2015).

[17] K. E. Aretouli, P. Tsipas, D. Tsoutsou, J. Marquez-Velasco, E. Xenogiannopoulou, S. A. Giamini, E. Vassalou, N. Kelaidis, and A. Dimoulas, Appl. Phys. Lett. **106**, 143105 (2015).

[18] W. Zhang, Z. Huang, W. Zhang, and Y. Li, Nano Res. **7**, 1731 (2014).

[19] M. Kang, S. Rathi, I. Lee, D. Lim, J. Wang, L. Li, M. A. Khan, and G.-H. Kim, Appl. Phys. Lett. **106**, 143108 (2015).

[20] L. F. Mattheiss, Phys. Rev. B **8**, 3719 (1973).

[21] R. Coehoorn, C. Haas, J. Dijkstra, C. J. F. Flipse, R. A. de Groot, and A. Wold, Phys. Rev. B **35**, 6195 (1987).

[22] R. H. Friend and A. D. Yoffe, Adv. Phys. **36**, 1 (1987).

[23] K. Rossnagel, New J. Phys. **12**, 125018 (2010).

[24] T. Eknapakul, P. D. C. King, M. Asakawa, P. Buaphet, R. H. He, S.-K. Mo, H. Takagi, K. M. Shen, F. Baumberger, T. Sasagawa, S. Jungthawan, and W. Meevasana, Nano Lett. **14**, 1312 (2014).

[25] A. Varykhalov, J. Sánchez-Barriga, A. M. Shikin, C. Biswas, E. Vescovo, A. Rybkin, D. Marchenko, and O. Rader, Phys. Rev. Lett. **101**, 157601 (2008).

[26] C. Riedl, C. Coletti, T. Iwasaki, A. A. Zakharov, and U. Starke, Phys. Rev. Lett. **103**, 246804 (2009).

[27] B. Ouyang, G. Lan, Y. Guo, Z. Mi, and J. Song, Appl. Phys. Lett. **107**, 191903 (2015).

[28] H. Fang, M. Tosun, G. Seol, T. C. Chang, K. Takei, J. Guo, and A. Javey, Nano Lett. **13**, 1991 (2013).

[29] A. Michail, N. Delikoukos, J. Parthenios, C. Galiotis, and K. Papagelis, Appl. Phys. Lett. **108**, 173102 (2016).

[30] A. Tarasov, S. Zhang, M. Y. Tsai, P. M. Campbell, S. Graham, S. Barlow, S. R. Marder, and E. M. Vogel, Adv. Mater. **27**, 1175 (2015).

[31] H. J. Conley, B. Wang, J. I. Ziegler, R. F. Haglund, S. T. Pantelides, and K. I. Bolotin, Nano Lett. **13**, 3626 (2013).

[32] Y. Ma, Y. Dai, M. Guo, C. Niu, Y. Zhu, and B. Huang, ACS Nano **6**, 1695 (2012).

[33] Y. Zhou, Z. Wang, P. Yang, X. Zu, L. Yang, X. Sun, and F. Gao, ACS Nano **6**, 9727 (2012).

[34] A. E. Maniadaki, G. Kopidakis, and I. N. Remediakis, Solid State Commun. **227**, 33 (2016).

[35] L. Brey, N. E. Christensen, and M. Cardona, Phys. Rev. B **36**, 2638 (1987).

[36] C. Priester, G. Allan, and M. Lannoo, Phys. Rev. B **37**, 8519 (1988).

[37] J. M. Riley, W. Meevasana, L. Bawden, M. Asakawa, T. Takayama, T. Eknapakul, T. K. Kim, M. Hoesch, S.-K. Mo, H. Takagi, T. Sasagawa, M. S. Bahramy, and P. D. C. King, Nat. Nanotechnol. **10**, 1043 (2015).

[38] Y. Zhang, T.-R. Chang, B. Zhou, Y.-T. Ciu, H. Yan, Z. Liu, F. Schmitt, J. Lee, R. Moore, Y. Chen, H. Lin, H.-T. Jeng, S.-K. Mo, Z. Hussain, A. Bansil, and Z.-X. Shen, Nat. Nanotechnol. **9**, 111 (2014).

[39] D. Le, A. Barinov, E. Preciado, M. Lsarraraz, I. Tanabe, T. Komesu, C. Troha, L. Bartels, T. S. Rahman, and P. A. Dowben, J. Phys.: Condens. Matter **27**, 182201 (2015).

[40] M. Silver, W. Batty, A. Ghiti, and E. P. O'Reilly, Phys. Rev. B **46**, 6781 (1992).

[41] X.-G. Zheng, H. Kuriyaki, and K. Hirakawa, J. Phys. Soc. Jpn. **58**, 622 (1989).

[42] S. Grimme, S. Ehrlich, and L. Goerigk, J. Comput. Chem. **32**, 1456 (2011).

[43] See Supplemental Material at http://link.aps.org/supplemental/10.1103/PhysRevB.97.201104 for the calculation of electronic bands under (i) electric field, (ii) doping and lattice deformation, and (iii) the fully relaxed atomic structure of $Na_{0.25}HfSe_2$.

[44] H. Yuan, M. S. Bahramy, K. Morimoto, S. Wu, K. Nomura. B.-J. Yang, H. Shimotani, R. Suzuki, M. Toh, C. Kloc, X. Xu, R. Arita, N. Nagaosa, and Y. Iwasa, Nat. Phys. **9**, 563 (2013).

[45] P. E. Blöchl, Phys. Rev. B **50**, 17953 (1994).

[46] J. P. Perdew, K. Burke, and M. Ernzerhof, Phys. Rev. Lett. **77**, 3865 (1996).

[47] J. P. Perdew, K. Burke, and M. Ernzerhof, Phys. Rev. Lett. **78**, 1396 (1997).

[48] X. Wang, X. Shen, Z. Wang, R. Yu, and L. Chen, ACS Nano **8**, 11394 (2014).

[49] D. Yang, S. J. Sandoval, W. M. R. Divigalpitiya, J. C. Irwin, and R. F. Frindt, Phys. Rev. B **43**, 12053 (1991).

[50] L. Bawden, J. M. Riley, C. H. Kim, R. Sankar, E. J. Monkman, D. E. Shai, H. I. Wei, E. B. Lochocki, J. W. Wells, W. Meevasana, T. K. Kim, M. Hoesch, Y. Ohtsubo, P. L. Fèvre, C. J. Fennie, K. M. Shen, F. Chou, and P. D. C. King, Sci. Adv. **1**, e1500495 (2015).

[51] A. Fathalian and J. Jalilian, Phys. Lett. A **374**, 4695 (2010).

[52] X. Peng and S. Velasquez, Appl. Phys. Lett. **98**, 023112 (2011).

[53] W. Wei, Y. Dai, and B. Huang, Phys. Chem. Chem. Phys. **19**, 663 (2017).

[54] Y. Jung, Y. Zhou, and J. J. Cha, Inorg. Chem. Front. **3**, 452 (2016).